

RESEARCH ARTICLE

10.1002/2015GB005267

Key Points:

- Global ocean carbon flux variability is simulated in a general circulation model
- Concentration gradient and transfer velocity control interannual flux variability
- Gas transfer velocity does not control pentadal North Atlantic flux variability

Supporting Information:

- Supporting Information S1
- Figure S1
- Figure S2
- Software S1
- Software S2
- Software S3
- Software S4
- Software S5
- Software S6
- Software S7
- Software S8
- Software S9
- Software S10
- Software S11
- Software S12
- Software S13

Correspondence to:

M. P. Couldrey,  
M.P.Couldrey@soton.ac.uk

Citation:

Couldrey, M. P., K. I. C. Oliver, A. Yool, P. R. Halloran, and E. P. Achterberg (2016), On which timescales do gas transfer velocities control North Atlantic CO<sub>2</sub> flux variability?, *Global Biogeochem. Cycles*, 30, 787–802, doi:10.1002/2015GB005267.

Received 15 AUG 2015

Accepted 12 APR 2016

Accepted article online 17 MAY 2016

Published online 31 MAY 2016

# On which timescales do gas transfer velocities control North Atlantic CO<sub>2</sub> flux variability?

Matthew P. Couldrey<sup>1</sup>, Kevin I. C. Oliver<sup>1</sup>, Andrew Yool<sup>2</sup>, Paul R. Halloran<sup>3</sup>, and Eric P. Achterberg<sup>1,4</sup>

<sup>1</sup>Ocean and Earth Science, University of Southampton, National Oceanography Centre, Southampton, UK, <sup>2</sup>National Oceanography Centre, Southampton, UK, <sup>3</sup>Geography, College of Life and Environmental Sciences, University of Exeter, Exeter, UK, <sup>4</sup>GEOMAR Helmholtz-Zentrum für Ozeanforschung, Kiel, Germany

**Abstract** The North Atlantic is an important basin for the global ocean’s uptake of anthropogenic and natural carbon dioxide (CO<sub>2</sub>), but the mechanisms controlling this carbon flux are not fully understood. The air-sea flux of CO<sub>2</sub>,  $F$ , is the product of a gas transfer velocity,  $k$ , the air-sea CO<sub>2</sub> concentration gradient,  $\Delta p\text{CO}_2$ , and the temperature- and salinity-dependent solubility coefficient,  $\alpha$ .  $k$  is difficult to constrain, representing the dominant uncertainty in  $F$  on short (instantaneous to interannual) timescales. Previous work shows that in the North Atlantic,  $\Delta p\text{CO}_2$  and  $k$  both contribute significantly to interannual  $F$  variability but that  $k$  is unimportant for multidecadal variability. On some timescale between interannual and multidecadal, gas transfer velocity variability and its associated uncertainty become negligible. Here we quantify this critical timescale for the first time. Using an ocean model, we determine the importance of  $k$ ,  $\Delta p\text{CO}_2$ , and  $\alpha$  on a range of timescales. On interannual and shorter timescales, both  $\Delta p\text{CO}_2$  and  $k$  are important controls on  $F$ . In contrast, pentadal to multidecadal North Atlantic flux variability is driven almost entirely by  $\Delta p\text{CO}_2$ ;  $k$  contributes less than 25%. Finally, we explore how accurately one can estimate North Atlantic  $F$  without a knowledge of nonseasonal  $k$  variability, finding it possible for interannual and longer timescales. These findings suggest that continued efforts to better constrain gas transfer velocities are necessary to quantify interannual variability in the North Atlantic carbon sink. However, uncertainty in  $k$  variability is unlikely to limit the accuracy of estimates of longer-term flux variability.

## 1. Introduction

Since the onset of the industrial era in the middle of the eighteenth century, human activities have altered oceanic and atmospheric chemistry, affecting the climate system. Fossil fuel consumption, changes in land use, and cement production rapidly release carbon as carbon dioxide (CO<sub>2</sub>) gas from geological reservoirs into the atmosphere, oceans, and terrestrial biosphere. This adds large amounts of “anthropogenic carbon” to the biogeochemically and/or radiatively active “natural carbon” pool. The effects of CO<sub>2</sub> on the Earth system are numerous and complex, but as a “greenhouse gas” it is a prominent control on climate [Myhre *et al.*, 2013]. Of the 555 ± 85 Pg of carbon emitted to the atmosphere between 1750 and 2011 by human activities, about half has remained in the atmosphere while 28% ± 5% has been taken up by the oceans, with the remainder taken up by the terrestrial biosphere [Ciais *et al.*, 2013].

The flux equation (1), describes the net exchange of CO<sub>2</sub> between the air and the ocean ( $F$ ). Here  $\Delta p\text{CO}_2$  is the disequilibrium between the partial pressures of CO<sub>2</sub> in the air and ocean ( $p\text{CO}_2^{\text{air}} - p\text{CO}_2^{\text{ocean}}$ ). Under this sign convention, an excess of CO<sub>2</sub> in the air gives positive  $\Delta p\text{CO}_2$  and  $F$ , driving exchange into seawater. If  $p\text{CO}_2^{\text{ocean}}$  is greater, outgassing occurs.  $p\text{CO}_2$  in seawater is primarily a function of temperature ( $T$ ), and dissolved inorganic carbon (DIC), but salinity ( $S$ ) and alkalinity also affect this. The gas transfer velocity,  $k$ , is a parameterization of how several aspects the physical environment enable CO<sub>2</sub> flux. Wind velocity is the main variable affecting  $k$  (increasing winds increases  $k$ ), but ice, surfactants, bubbles, and other factors also play important roles [Wanninkhof *et al.*, 2009]. The Schmidt number (the ratio between kinematic viscosity and molecular diffusion) also affects  $k$ , varying with water temperature.  $\alpha$  is Henry’s constant of CO<sub>2</sub> solubility in seawater [Weiss, 1974], quantifying how temperature, salinity, and pressure affect solubility.

$$F = \Delta p\text{CO}_2 \times k \times \alpha \tag{1}$$

CO<sub>2</sub> flux is difficult to measure directly due to the need for high temporal resolution measurements of  $p\text{CO}_2$  and small-scale turbulence [McGillis *et al.*, 2001], and so a more common approach is to measure or estimate each quantity on the right-hand side (RHS) of equation (1).  $\alpha$  is the most straightforward to determine, varying primarily with temperature and also with salinity.  $\alpha$ 's contribution to flux variability is generally well constrained and found to be minor on interannual timescales [e.g., Doney *et al.*, 2009].  $\Delta p\text{CO}_2$  and  $k$ , however, present distinct challenges for ocean carbon research. The primary challenge with studying global  $\Delta p\text{CO}_2$  variability is to place as many measurement systems in as many locations as possible and to maintain those observations through time. The Surface Ocean CO<sub>2</sub> Atlas (SOCAT) is an example of a global effort to compile measurements of ocean surface CO<sub>2</sub> gathered by autonomous underway systems on commercial vessels and research cruises [Bakker *et al.*, 2014].

The main difficulties in quantifying gas transfer velocity stem from its dependence on several elements of the physicochemical environment. The main variable used to derive a gas transfer velocity is wind speed, but  $k$  is also dependent on the smoothness of the sea surface (i.e., the presence of breaking and nonbreaking waves [Frew *et al.*, 2007]), bubble entrainment, rain, buoyancy-generated turbulence, surfactants, and other factors [Wanninkhof *et al.*, 2009]. Given the large range of variables, and poor constraints of their effects on  $k$ , field measurement of gas transfer velocity is difficult. In attempts to refine these uncertainties, several parameterizations have been proposed, derived using a number of techniques, but there is no consensus which is the most accurate [Bender *et al.*, 2011]. Instead, authors tend to attempt to quantify  $k$  uncertainty in two ways: the uncertainty inherent to a particular parameterization (resulting from the spread of data points about the polynomial fitted) and the variation in derived  $k$  from the use of different parameterizations. Published uncertainties relating to  $k$  are often not statistically sound and represent ad hoc best estimates of error [Wanninkhof, 2014]. The result is that considerable CO<sub>2</sub> flux uncertainty originates from uncertainties in the gas transfer velocity.

While the whole global ocean represents a large net sink of CO<sub>2</sub> for the atmosphere, its uptake is not uniform spatially or temporally. The tropical oceans are net CO<sub>2</sub> outgassing regions, whereas at higher latitudes there is net uptake by seawater [Takahashi *et al.*, 2009; Landschützer *et al.*, 2014]. The major upwelling regions are outgassing zones, and the strongest sites of ocean CO<sub>2</sub> uptake are areas of deep water formation. In the North Atlantic, the combination of deep water formation and high biological carbon fixation creates ideal physical and biogeochemical conditions for strong ocean CO<sub>2</sub> uptake, distinguishing it from other basins [Sabine *et al.*, 2004; Khatiwala *et al.*, 2009]. It is therefore an important focus region in the ocean carbon cycle.

The evolution of the North Atlantic carbon sink on decadal and longer timescales is unclear, yet its quantification is necessary for future climate change prediction [Halloran *et al.*, 2015]. Bates [2007] and Takahashi *et al.* [2009] call attention to this gap in knowledge, highlighting that a major limitation to our ability to understand this variability stems from limited spatiotemporal coverage of CO<sub>2</sub> observations. Although data sets with large spatial coverage exist (e.g., SOCAT [Bakker *et al.*, 2014]), they lack the temporal duration required to study long timescales [Halloran *et al.*, 2015]. Equally, the long-time series sites with sufficient data to quantify multiannual variability, such as the Bermuda Atlantic Time Series (BATS) and others reviewed recently by Bates *et al.* [2014], may not necessarily represent the systems at the basin scale [McKinley *et al.*, 2004]. Given these temporal and spatial data gaps, numerical modeling studies provide unique insight into an incompletely observed system.

It is necessary to understand where observational uncertainties limit our ability to confidently predict future climate change. Previous work investigating global ocean carbon flux interannual variability has found both  $\Delta p\text{CO}_2$  and  $k$  to be important drivers [Doney *et al.*, 2009; Long *et al.*, 2013]. Other work has found that North Atlantic multidecadal CO<sub>2</sub> flux variability is controlled chiefly by the contribution from  $\Delta p\text{CO}_2$  [McKinley *et al.*, 2011]. Therefore, on these multidecadal timescales, uncertainty in gas transfer velocity variability does not considerably limit estimates of flux variability, because the contribution from  $k$  is minor. On some intermediate critical timescale between interannual and multidecadal, flux variability transitions from a regime that is  $k$  and  $\Delta p\text{CO}_2$  controlled to purely  $\Delta p\text{CO}_2$  controlled. Presently, neither the magnitude of this critical timescale nor its spatial structure is known, yet both are needed to understand where uncertainties in  $\Delta p\text{CO}_2$  and  $k$  add uncertainty in derived fluxes.

Here we attribute CO<sub>2</sub> flux variability to contributions from all flux equation components on a range of timescales, to identify the timescales where  $k$  becomes unimportant. We hypothesize that on interannual and shorter timescales, both  $k$  and  $\Delta p\text{CO}_2$  will be important in controlling flux variability but that for longer-term variability,  $\Delta p\text{CO}_2$  will be the dominant contributor. We examine 150 years of ocean biogeochemical model

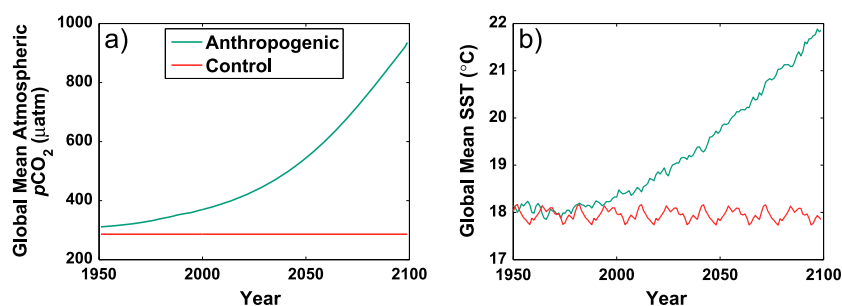


**Figure 1.** Annual mean (a) atmospheric  $p\text{CO}_2$  and (b) sea surface temperature (SST) for the anthropogenic (green) and control (red) runs, for 1950–2099 (model year 1 is 1860).

output, forced with two scenarios: (1) sharply rising, following historical measurements and RCP8.5 [Riahi *et al.*, 2011], and (2) fixed preindustrial atmospheric  $\text{CO}_2$  concentrations. First, we determine that our setup is appropriate to test our hypothesis, comparing observed and modeled variability. Next, we compare our model's representation of interannual flux variability with those of previous studies, before expanding our methodology to examine more specific timescales of variability. We then identify which long timescales of flux variability, if any, are driven entirely by the  $\Delta p\text{CO}_2$  contribution, with negligible influence from  $k$ . Finally, we examine how successfully one can estimate flux variability with only a very limited knowledge of the contribution of  $k$ .

## 2. Methods

### 2.1. Model Setup

We investigate the controls of ocean carbon flux variability on different timescales using a numerical ocean general circulation model (GCM), version 3.2 of the Nucleus for European Modelling of the Ocean (NEMO) physical ocean model [Madec, 2008]. This model includes sea ice, version 2 of the Louvain-la-Neuve Ice Model (LIM2) [Timmermann *et al.*, 2005]. NEMO was run with a  $1^\circ$  horizontal resolution using the ORCA-1 grid [Madec and Imbard, 1996]. This grid is not sufficient to resolve the mesoscale but has a finer scale of about  $1/3^\circ$  of latitude at the equator to better represent equatorial upwelling. The grid has  $292 \times 362$  horizontal points and 64 vertical levels (with smaller spacing at the surface, increasing with depth).

NEMO is coupled with an intermediate-complexity ecosystem model, MEDUSA 2.0 [Yool *et al.*, 2013a]. MEDUSA 2.0 separately simulates “large” organisms (mesozooplankton and microphytoplankton like diatoms) and “small” ecosystem members (to represent the microbial loop). MEDUSA 2.0 resolves nitrogen, silicon, iron, carbon, alkalinity, and oxygen cycles. The model includes representations of sinking of detrital matter and benthic interactions. The Nightingale *et al.* [2000] gas transfer velocity parameterization is used, with the Schmidt number of Wanninkhof [1992]. This parameterization is commonly used as it is considered to be one of the more robust; the function shows a high proportion (82%) of the variance of dual-tracer release data explained by wind speed [Ho *et al.*, 2011].

Output from the HadGEM2-ES Earth System Model is used as the atmospheric forcing set [Yool *et al.*, 2013b]. HadGEM2-ES includes physical models of the ocean and atmosphere, the terrestrial and ocean carbon cycles, tropospheric chemistry, and aerosols [Collins *et al.*, 2011]. The surface fluxes of heat, momentum and freshwater, and atmospheric chemistry from HadGEM2-ES were used to force NEMO at 6-hourly intervals. The atmospheric forcing set for the “anthropogenic” run prescribes concentrations of atmospheric  $\text{CO}_2$  (and other greenhouse gases: methane, nitrous oxide, and halocarbons) following RCP8.5 [Jones *et al.*, 2011]. RCP8.5 is a high greenhouse gas emissions scenario, with atmospheric  $p\text{CO}_2$  exceeding 900 ppm by the year 2100 [Riahi *et al.*, 2011] (Figure 1a, green curve). This prescribed anthropogenic source of greenhouse gases into the atmosphere affects the radiative forcing balance and causes a net rise in global temperatures, including sea surface temperature (SST) (Figure 1b). The integration was run for 240 years.

A control run was also generated using a very similar setup to the experimental run, except with a different atmospheric  $p\text{CO}_2$  scenario. In this run, atmospheric  $p\text{CO}_2$  is held at a preindustrial value of 286 ppmv (Figure 1a, red curve). Only 30 years of this forcing set (i.e., output from HadGEM2-ES run with fixed preindustrial atmospheric  $\text{CO}_2$ ) were available to force NEMO-MEDUSA. Therefore, to obtain a comparable 240 year control run, NEMO-MEDUSA was forced with eight repetitions of the forcing set. The control provides insight

into the system's internal variability, without forced changes in the radiation budget (observable in global mean SST: Figure 1b) and global biogeochemistry. Internal variability in the control run on timescales longer than 30 years is evident (e.g., in atmospheric  $p\text{CO}_2$  and SST, Figure 1, red curves), but given the forcing setup of this run, it is not included in our analysis.

## 2.2. Decomposition of $\text{CO}_2$ Flux Variability

To explore the drivers behind  $\text{CO}_2$  flux variability, we use a Reynolds decomposition to separate the time-varying ( $y'$ ) and time mean ( $\bar{y}$ ) components of monthly averaged model output, as in equation (2). The time-varying component is therefore the monthly anomaly from a time mean, representing nonseasonal variability.

$$y = y' + \bar{y} \quad (2)$$

The flux of  $\text{CO}_2$  is the product of three variables, equation (1). Therefore, a Reynolds decomposition for three forcing components is needed. The generalized decomposition for three components and its expansion is shown in equations (3)–(5), where  $a$ ,  $b$ , and  $c$  are the forcing components, corresponding to the three RHS variables in equation (1).

$$y = abc \quad (3)$$

$$y' + \bar{y} = (a' + \bar{a})(b' + \bar{b})(c' + \bar{c}) \quad (4)$$

$$= \bar{a}\bar{b}\bar{c} + a'\bar{b}\bar{c} + \bar{a}b'\bar{c} + \bar{a}\bar{b}c' + \bar{a}b'c' + a'\bar{b}c' + a'b'\bar{c} + a'b'c' \quad (5)$$

The time mean component,  $\bar{y}$ , is time mean of each of the RHS terms in equation (5), as in equation (6). Terms in equation (6) containing the time means of two forcing components ( $\overline{a'b\bar{c}}$ ,  $\overline{\bar{a}b'c}$ , and  $\overline{\bar{a}\bar{b}c'}$ ) always have values of zero, giving equation (7).

$$\bar{y} = \overline{\bar{a}\bar{b}\bar{c}} + \overline{a'\bar{b}\bar{c}} + \overline{\bar{a}b'\bar{c}} + \overline{\bar{a}\bar{b}c'} + \overline{\bar{a}b'c'} + \overline{a'\bar{b}c'} + \overline{a'b'\bar{c}} + \overline{a'b'c'} \quad (6)$$

$$= \overline{\bar{a}\bar{b}\bar{c}} + \overline{\bar{a}b'c'} + \overline{a'b'\bar{c}} + \overline{a'b'c'} \quad (7)$$

We subtract  $\bar{y}$  from both sides of equation (5) to solve for the time-varying component of  $y$ , equations (8) and (9). This gives an expression for  $y'$  in terms of the contributions from separate components, equation (10). Note that  $\overline{\bar{a}\bar{b}\bar{c}} = \overline{\bar{a}\bar{b}\bar{c}}$ , so the difference between the two terms cancels to zero in equation (10).

$$y' = y - \bar{y} \quad (8)$$

$$= (\bar{a}\bar{b}\bar{c} + a'\bar{b}\bar{c} + \bar{a}b'\bar{c} + \bar{a}\bar{b}c' + \bar{a}b'c' + a'\bar{b}c' + a'b'\bar{c} + a'b'c') - (\overline{\bar{a}\bar{b}\bar{c}} + \overline{\bar{a}b'c'} + \overline{a'b'\bar{c}} + \overline{a'b'c'}) \quad (9)$$

$$= a'\bar{b}\bar{c} + \bar{a}b'\bar{c} + \bar{a}\bar{b}c' + (a'b'c' - \overline{a'b'c'}) + (a'b'\bar{c} - \overline{a'b'\bar{c}}) + (a'\bar{b}c' - \overline{a'\bar{b}c'}) + (\bar{a}b'c' - \overline{\bar{a}b'c'}) \quad (10)$$

We arrive at an equation for flux anomalies by expressing anomalies in the flux equation (1) using the expansion in equation (10):

$$F' = \underbrace{\Delta p\text{CO}_2' \bar{k} \bar{\alpha}}_{\text{term1}} + \underbrace{\overline{\Delta p\text{CO}_2' k' \bar{\alpha}}}_{\text{term2}} + \underbrace{\overline{\Delta p\text{CO}_2' \bar{k} \alpha'}}_{\text{term3}} + \underbrace{(\Delta p\text{CO}_2' k' \bar{\alpha} - \overline{\Delta p\text{CO}_2' k' \bar{\alpha}})}_{\text{term4}} + \underbrace{(\Delta p\text{CO}_2' \bar{k} \alpha' - \overline{\Delta p\text{CO}_2' \bar{k} \alpha'})}_{\text{term5}} \\ + \underbrace{(\overline{\Delta p\text{CO}_2' k' \alpha'} - \overline{\Delta p\text{CO}_2' k' \alpha'})}_{\text{term6}} + \underbrace{(\Delta p\text{CO}_2' k' \alpha' - \overline{\Delta p\text{CO}_2' k' \alpha'})}_{\text{term7}} \quad (11)$$

The physical interpretation of these terms is the anomaly in  $\text{CO}_2$  flux from a long-term monthly mean produced by variability in  $\Delta p\text{CO}_2$  (term 1), in  $k$  (term 2), and in  $\alpha$  (term 3) and through nonlinear interactions between components (terms 4 to 7). Rather than consider each of the cross terms (terms 4 to 7) in equation (11) separately, we consider their sum as one term. This is because the role of the cross terms (even when added together) in controlling  $F'$  is minor, demonstrated in section 4.1. When summed, the decomposed contributions reliably reconstruct monthly mean fluxes, suggesting that the decomposition is not compromised by covariances between components of the flux equation and synoptic-scale variability.

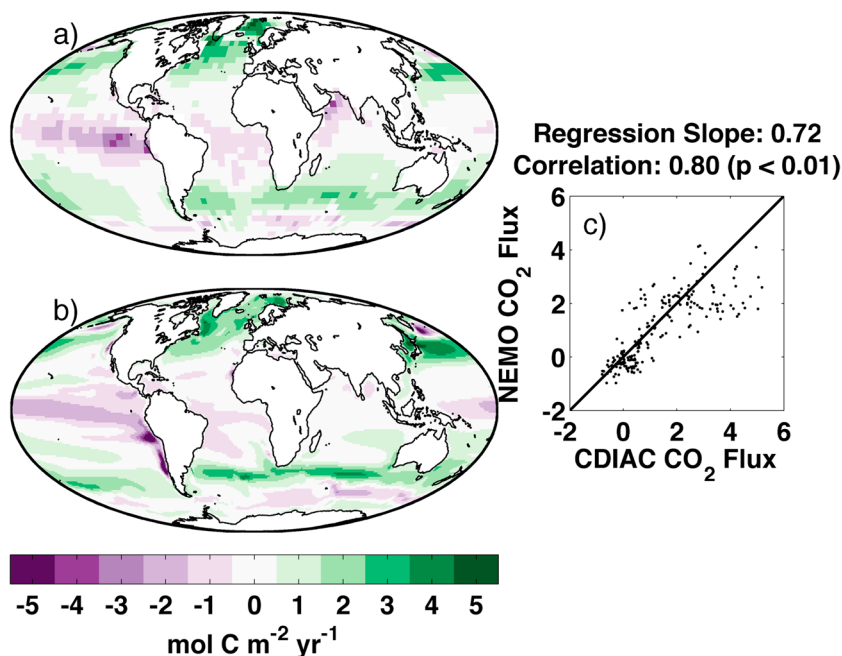


**Figure 2.** (a) LDEO climatological flux of CO<sub>2</sub> into the ocean for the reference year 2000, positive values indicating ocean uptake of gas [Takahashi *et al.*, 2009]. (b) Modeled mean CO<sub>2</sub> flux over 1995–2005 for the anthropogenic run. (c) LDEO versus modeled North Atlantic climatological CO<sub>2</sub> flux (mol C m<sup>-2</sup> yr<sup>-1</sup>).

To investigate how much each term in equation (11) contributes to variability in  $F'$ , we regress the values of terms 1–3 at each grid point for each month against the monthly flux anomaly at that grid point. This method is detailed further by Doney *et al.* [2007] and Doney *et al.* [2009]. For example, to solve for the change in  $y'$  due to the first forcing component  $a'\bar{b}\bar{c}$ , we regress the former against the latter:

$$\frac{\partial y'}{\partial a'\bar{b}\bar{c}} = \beta_a \quad (12)$$

This yields a slope,  $\beta$ , which quantifies how strongly a given RHS term in equation (11) contributes to anomalies in the CO<sub>2</sub> flux. In equation (12), the subscripted  $a$  denotes that in this example,  $\beta_a$  signifies the change in  $y'$  with respect to variability in the forcing component,  $a$ .  $\beta$  close to one indicates that a term contributes strongly to the value of  $F'$ , whereas a slope of 0 shows that  $F'$  is insensitive to that term. Values of  $\beta$  may be less than 0 if a term is anticorrelated with  $F'$ . In such cases, one or more terms will have slopes greater than 1 to compensate for a different  $\beta$  being smaller than 0. In general,  $\sum \beta = 1$  (i.e., the linearity assumption of the regression) does not hold due to cross correlations, but we find that the sum of all slopes is predominantly in the range  $0.8 < \sum \beta < 1$ . This suggests that the assumption of linearity in the response of  $y'$  to its predictors is effectively met.

### 3. Validation

Previous work has compared output from MEDUSA 2.0 to biogeochemical observations on global and regional scales in more detail [Yool *et al.*, 2013a], which we briefly summarize before elaborating our own validation. In general, the model captures much of the spatial and seasonal patterns of primary productivity but shows a low bias in the subtropics, a high bias in high-nutrient/low-chlorophyll regions, and underestimates the strength of the North Atlantic spring bloom. MEDUSA 2.0 tends to show “higher highs” of surface DIC than the GLODAP [Takahashi *et al.*, 2009] fields [Yool *et al.*, 2013a, Figure 16], but the broader spatial patterns are well reproduced. Similarly, air-sea  $\Delta p\text{CO}_2$  seasonal highs and lows are somewhat exaggerated, particularly the North Atlantic winter [Yool *et al.*, 2013a, Figures 21 and 22]. While these findings are useful to bear in mind, our study focuses on carbon flux variability on interannual and longer timescales that has not been thoroughly validated.

We first assess the ability of our setup to reproduce the major spatial features of the climatological CO<sub>2</sub> flux by comparing observational time mean fluxes [the Lamont-Doherty Earth Observatory or LDEO flux climatology

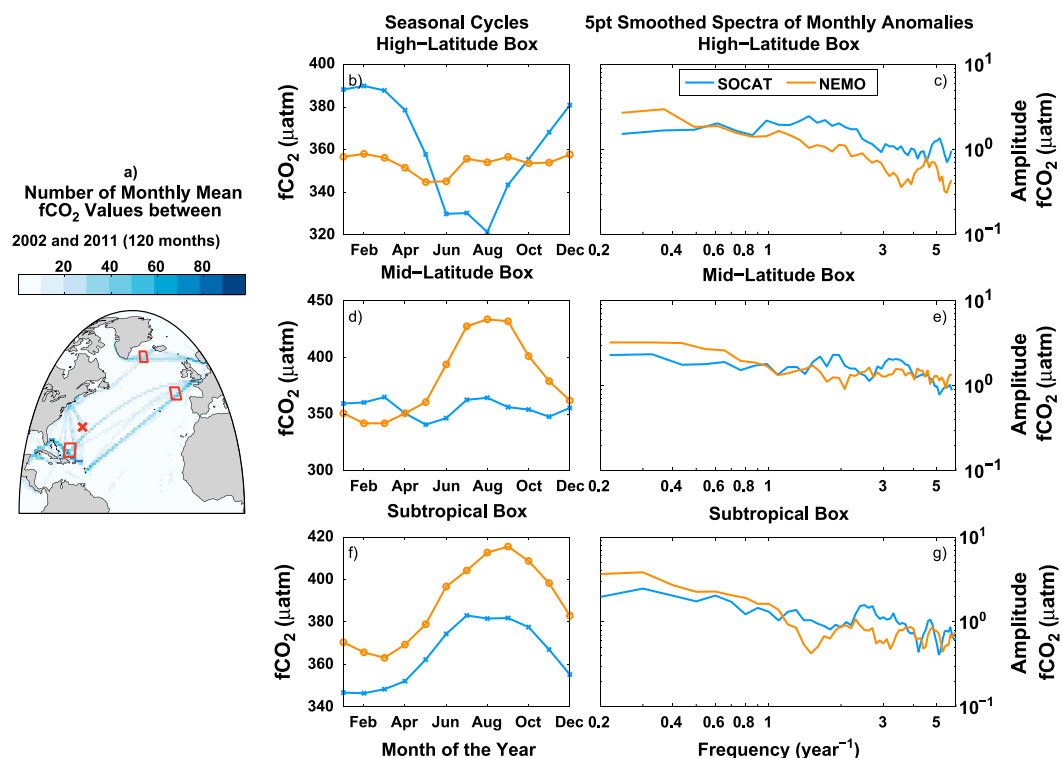


**Figure 3.** Comparison of data from the SOCAT database and output from the anthropogenic run. (a) Coverage of SOCAT monthly mean  $f\text{CO}_2$  values 2002–2011, red squares: locations of comparison regions, red cross: location of BATS site. (b, d, and f) Monthly mean  $f\text{CO}_2$  climatologies for the three comparison regions (high latitude, midlatitude, and subtropical, respectively) for 2002–2011: for SOCAT (blue) and NEMO-MEDUSA (orange). (c, e, and g) Frequency spectra of monthly  $f\text{CO}_2$  anomalies, smoothed with a five-point running mean.

[Takahashi *et al.*, 2009] with model output (Figure 2). The most prominent large-scale features are well represented in our model: low-latitude efflux and high-latitude influx. Some of the largest discrepancies between the model and observations occur in the South Pacific, where measurements are sparse. For the purposes of our study, these differences are unimportant, since we focus on the North Atlantic. After interpolating the model North Atlantic  $\text{CO}_2$  flux climatology onto the coarser grid of the Takahashi observational climatology, the two can be compared quantitatively. The North Atlantic climatological  $\text{CO}_2$  flux is one of the best represented basins in our setup; here the model somewhat underestimates high values of flux, but otherwise, the two are well correlated (with a correlation coefficient  $r$  value of 0.80,  $p < 0.01$ ) (Figure 2c).

Next, we attempt to validate the model's temporal variability. Direct  $\text{CO}_2$  flux observations representing large spatial and temporal scales do not exist, so instead, we validate our model's  $f\text{CO}_2$  fields ( $\text{CO}_2$  fugacity is almost equivalent to  $p\text{CO}_2$  but is scaled for the nonideal nature of real-world gases). We compare our model output against (1) the SOCAT database of surface  $f\text{CO}_2$  observations (which maximizes spatial coverage at the expense of temporal length) [Bakker *et al.*, 2014] and (2) data collected at the BATS site (to compare variability on the longest timescale possible, although only for a limited area). We compare fields of  $f\text{CO}_2$  rather than  $\Delta p\text{CO}_2$  because in our setup, the atmospheric  $p\text{CO}_2$  only varies with the increase prescribed under RCP8.5, and so all of the modeled  $\Delta p\text{CO}_2$  variability arises from the oceanic side. Spatial and temporal (other than the trend) variability in atmospheric  $p\text{CO}_2$  are omitted in our setup but are small (order 1–10 ppm) in comparison to the oceanic  $p\text{CO}_2$  variability of interest (order 10–100 ppm) [Wanninkhof *et al.*, 2013].

We compare our model output with  $1 \times 1^\circ$  monthly mean gridded  $f\text{CO}_2$  fields from the SOCAT database (version 2) [Bakker *et al.*, 2014]. For this comparison, we first regrid our model output onto the SOCAT grid. Although the data set includes values from the 1970s, the most consistent temporal coverage in the North Atlantic is between 2002 and 2011. We choose three locations in zonally distinct regions on the basis that they had the most complete set of observations for this period. We select data from  $5 \times 5^\circ$  areas across the North Atlantic (subtropical: northeast of the Caribbean, midlatitude: east of the Bay of Biscay, and high

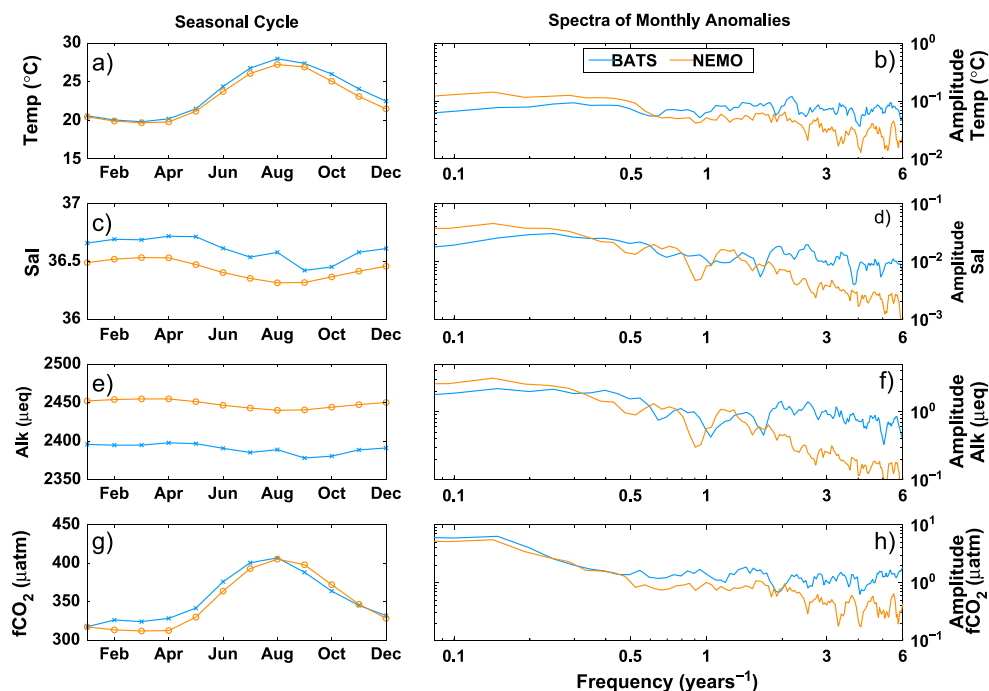


**Figure 4.** Comparison of (a and b) temperature, (c and d) salinity, (e and f) alkalinity, and (g and h)  $f\text{CO}_2$  from BATS, Bermuda (blue), with corresponding NEMO-MEDUSA anthropogenic run output (orange). Figures 4a, 4c, 4e, and 4g show climatological monthly means for 1991–2011. Figures 4b, 4d, 4f, and 4h show five-point smoothed frequency spectra of monthly anomalies for 1991–2011.

latitude: south of Greenland/Iceland) to compare against our model output (Figure 3a, orange boxes). The comparison is insensitive to the exact location of the boxes (shifting their positions by a few degrees gives similar results) and the time period of model output used. It was not possible to apply this comparison to the equatorial Atlantic, as there were insufficient monthly mean  $f\text{CO}_2$  values (Figure 3a). We calculate a monthly climatology of time mean  $f\text{CO}_2$  fields (Figures 3b, 3d and 3f) and monthly anomalies from this climatology for the 2002–2011 period. We then calculate frequency spectra of the  $f\text{CO}_2$  anomalies for each box (Figures 3c, 3e, and 3g). Data gaps were filled with that month's mean value, plus the contribution of the linear trend. Where gaps existed in the SOCAT data, the model output was accordingly subsampled and the resulting gaps were filled in the same way as for the observations.

Clear differences exist between the modeled and observed seasonal cycles of  $f\text{CO}_2$  (Figures 3b, 3d, and 3f). These differences are unimportant for our study, which does not focus on seasonal variability. The comparison between the frequency spectra of the model output and the observations is similar across all boxes: high-frequency (short-timescale) variability is similar or slightly higher in observations, and low frequencies (long timescales) show slightly more energy in the model. The discrepancies at high frequencies are unsurprising, as the observations will reflect features that are unresolved by the model, such as mesoscale eddies. Although the  $f\text{CO}_2$  variability at low frequencies is larger in the model, the agreement with observations is within a factor of 2.

The carbon system data collected at BATS, Bermuda (64°W, 31.5°N), are among the longest and most consistent, covering the years 1991 to 2011. The seasonal cycle amplitudes of all four parameters are well resolved in the model, with systematic offsets in salinity and alkalinity (Figures 4c and 4e). Nonseasonal variability is well represented (Figures 4b, 4d, 4f, and 4h). As with the SOCAT-NEMO comparison, there is substantial high-frequency variability in the observations not present in the model output, since the former represents snapshots of real-world features, while the latter represents monthly mean output from a  $1 \times 1^\circ$  model grid cell. Overall, the model tends to underestimate subannual variability but captures the amplitudes on longer timescales that are relevant for this study.

The gas transfer velocity is primarily a function of wind speed, so it is important that our setup reproduces realistic wind fields and variability. Other work has explored the performance of the HadGEM2 models more

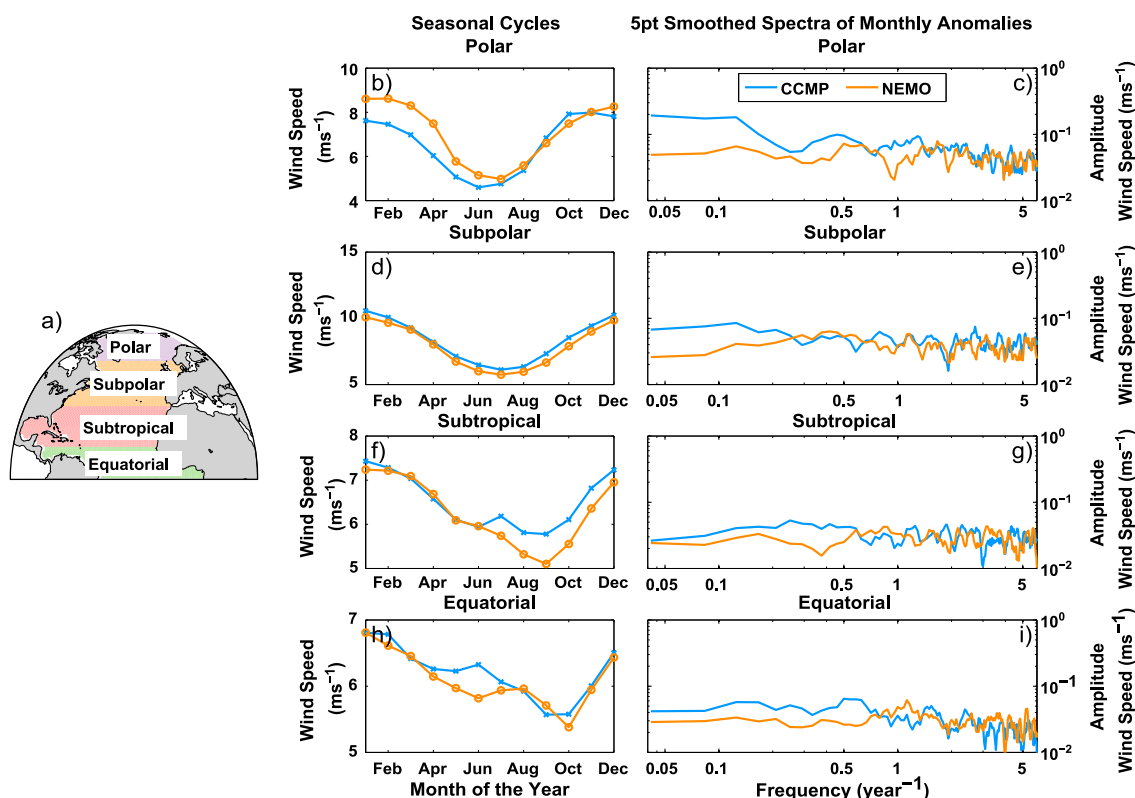


**Figure 5.** Comparison of wind variability from the CCMP wind product [Atlas *et al.*, 2011] and the anthropogenic run. (a) Division of zones. (b, d, f, and h) Monthly mean wind speed climatologies for the four zonal areas (polar, subpolar, subtropical, and equatorial, respectively) for 1988–2011: for CCMP (blue) and NEMO-MEDUSA (orange). (c, e, g, and i) Frequency spectra of monthly wind speed anomalies, smoothed with a five-point running mean.

generally [Martin *et al.*, 2011; Collins *et al.*, 2011]. We compare the wind fields used to force NEMO-MEDUSA with monthly mean Cross-Calibrated Multiplatform (CCMP) sea surface (10 m) winds [Atlas *et al.*, 2011], which cover the period 1988–2011. CCMP zonal wind speed variability is similar to other products [Wanninkhof *et al.*, 2013], and so our comparison would likely produce similar results if other wind data sets were chosen. We regrid the data from its  $0.25 \times 0.25^\circ$  grid onto a  $1 \times 1^\circ$  grid for comparison with our model output. We construct a monthly climatology and fields of anomalies of wind speeds. Similarly to the other aspects of the validation, we construct frequency spectra of the model and observation anomaly fields (Figure 5). In general, agreement between the model and observations is good for variability with frequencies higher than  $0.25 \text{ year}^{-1}$  and somewhat poorer for lower frequencies (longer timescales). In the subpolar and polar North Atlantic, the model underestimates low-frequency wind variability.

## 4. Results

### 4.1. The Roles of Flux Components in Interannual Variability

In this section, we investigate the drivers behind interannual  $\text{CO}_2$  flux variability, quantifying the contributions of its components,  $\Delta p\text{CO}_2$ ,  $k$ , and  $\alpha$ . This approach builds on the methodology of Doney *et al.* [2009], attributing interannual flux variability to each component. First, we establish that our model setup is able to represent  $\text{CO}_2$  flux variability comparable to previous estimates using the portion of the simulation which overlaps the observational record.

To assess global  $\text{CO}_2$  flux interannual variability, we calculate the root-mean-square (RMS) or standard deviation of globally integrated monthly flux anomalies. From monthly averaged  $\text{CO}_2$  flux fields at each grid point, we subtract a long-term mean flux (spanning 1980–2009) for each month to generate anomaly fields. For this time period, variability is insensitive to the choice of RCP because the scenarios have not yet substantially diverged [Myhre *et al.*, 2013]. We globally integrate those flux anomalies and calculate the square root of the mean squared anomaly, yielding the RMS. The metric is quite sensitive to the duration over which it is calculated. We calculate the RMS over a similar time period to other studies (1980 to 2009), finding a value

**Table 1.** Comparison of Global Interannual Variability (RMS or Standard Deviation of Monthly CO<sub>2</sub> Flux Anomalies) From Various Studies

Variability (Pg C yr <sup>-1</sup> )	Approach	Time Period	Reference
0.20	Model	1979–1997	<i>Le Quéré et al.</i> [2000]
0.23	Model	1961–1998	<i>Obata and Kitamura</i> [2003]
0.28	Model	1980–1998	<i>McKinley et al.</i> [2004]
0.34	Model	1979–2004	<i>Doney et al.</i> [2009]
0.20	Observation and Model	1990–2009	<i>Wanninkhof et al.</i> [2013]
0.31	Observations	1993–2008	<i>Rödenbeck et al.</i> [2014]
0.12	Observations	1998–2011	<i>Landschützer et al.</i> [2014]
0.29	Model	1980–2009	This Study

of 0.29 Pg C yr<sup>-1</sup>, comparable to previous estimates (Table 1). Two recent observational estimates of interannual flux variability differ by a factor of 2 [Rödenbeck et al., 2014; Landschützer et al., 2014], which the authors attribute to differing time periods of study. Landschützer et al. [2014] comment that their data do not cover the strong 1997/1998 El Niño period, which made the Rödenbeck et al. [2014] estimate much larger.

Qualitatively, our setup captures many of the key regional hot spots of interannual variability between 1980 and 2009 (Figure 6a): the equatorial Pacific, the subpolar and subtropical oceans, and the south Southern Ocean [e.g., Doney et al., 2009; Rödenbeck et al., 2014]. The North Atlantic is a notable region for its large interannual CO<sub>2</sub> flux variability. The areas with the strongest variability (>1.0 mol m<sup>-2</sup> yr<sup>-1</sup>) are in the subpolar gyre, along the sea ice edge of the Labrador Sea, along the Greenland coast, and along the path of the North Atlantic Current (NAC). The subtropical gyre shows a relatively moderate level of variability (up to 1 mol m<sup>-2</sup> yr<sup>-1</sup>) which decays with distance from the NAC. The equatorial Atlantic shows the lowest overall CO<sub>2</sub> flux variability.

To investigate the causes of the interannual variability illustrated in Figure 6a, we estimate the contribution of each component of the flux equation (1) using the linear expansion of  $F'$  (equation (11)). At each grid point for all months, we calculate the contribution of each term in equation (11). Taking each of these contributions, we regress them against the grid point's monthly CO<sub>2</sub> flux anomalies ( $F'$ ) to quantify the influence of that particular term on  $F'$ , as in equation (12). This allows us to compare the contributions of  $\Delta p\text{CO}_2$ ,  $k$ ,  $\alpha$ , and the cross terms (Figures 6b–6e, respectively) to variability in  $F'$ .

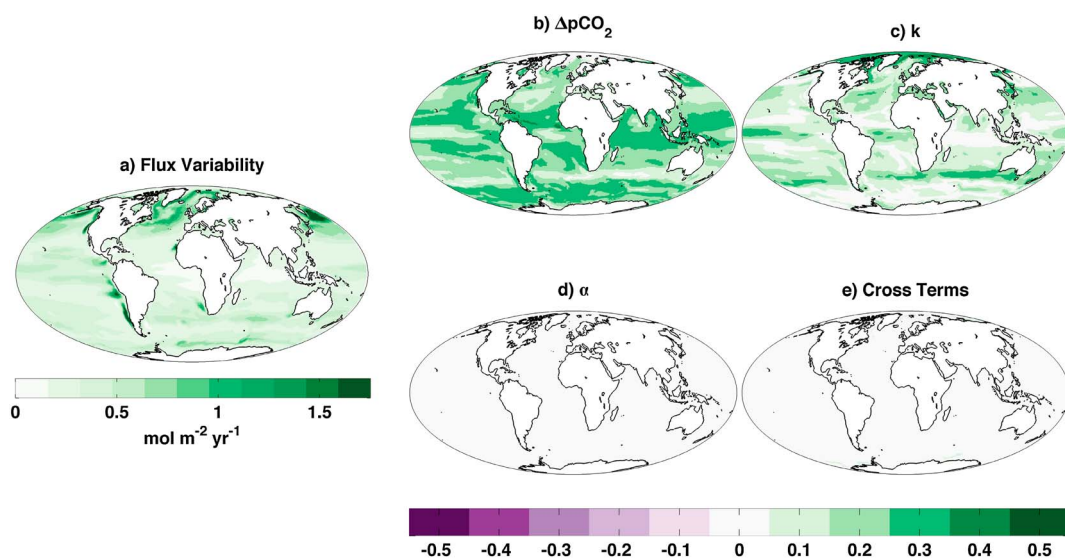


**Figure 6.** (a) Interannual CO<sub>2</sub> flux variability as the RMS of deseasonalized monthly anomalies and contributions of (b)  $\Delta p\text{CO}_2$ , (c)  $k$ , (d)  $\alpha$ , and (e) cross terms to interannual variability in the CO<sub>2</sub> flux for the period 1980–2009 of the anthropogenic run, as in equation (12).

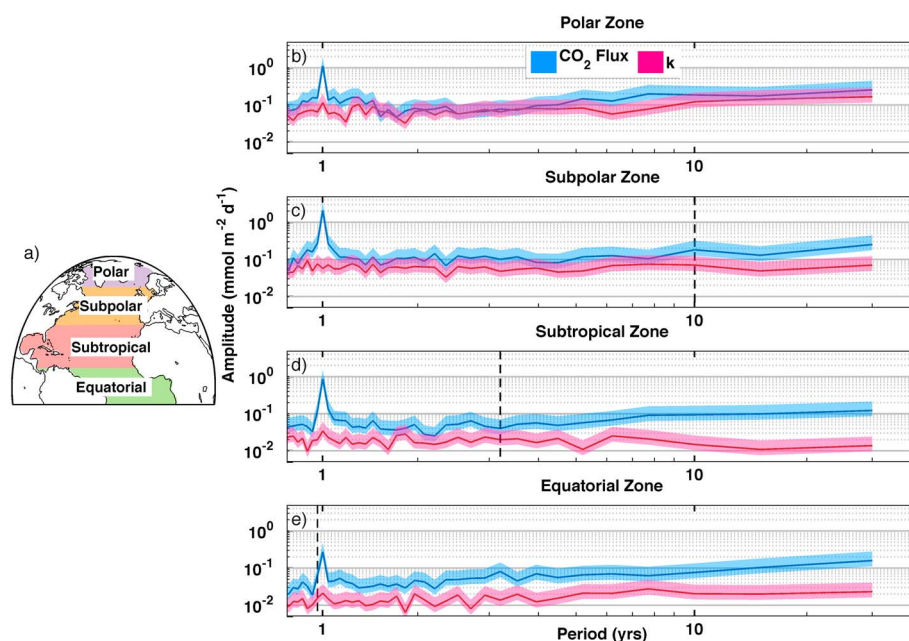


**Figure 7.** (a) North Atlantic zones and their period spectra of zonally averaged  $\text{CO}_2$  flux (blue) and (b–e) the contribution to flux variability from  $k$  (red) for the anthropogenic run, 1950–2009. The dark colored lines denote best estimates of spectra, and lighter shaded regions show the spectra within 95% confidence. Vertical dashed lines indicate the critical timescale: the shortest timescale that for all longer timescales, the best estimate of  $\text{CO}_2$  flux variability is at least twice as large as that of  $k$ .

Over much the global ocean,  $\Delta p\text{CO}_2$  is the most important contributor to interannual  $\text{CO}_2$  flux variability (Figure 6b), in agreement with the findings of *Doney et al.* [2009]. The global area-weighted mean  $\Delta p\text{CO}_2$  contribution is  $0.20 \text{ mol m}^{-2} \text{ yr}^{-1}$ , about 60% of the global interannual  $\text{CO}_2$  flux variability. The role of  $k$  is also important in almost all regions, contributing about 35% of global interannual flux variability, but is the most significant where the role of  $\Delta p\text{CO}_2$  is smaller (Figure 6c). Indeed, Figures 6b and 6c mirror each other, since nearly all interannual variability in the  $\text{CO}_2$  flux comes from variability in either  $\Delta p\text{CO}_2$  or  $k$ . This is because the contributions from  $\alpha$  and the cross terms are minor (Figures 6d and 6e). Furthermore, most of the variability observed when considering  $k$  and  $\alpha$  together as one component comes from  $k$ , as was assumed by *Doney et al.* [2009].

Many of the locations where  $k$  is an important driver behind interannual  $\text{CO}_2$  flux variability coincide with the edges of the seasonally ice-covered oceans. This is because  $k$  is scaled by the proportion of each ocean grid cell area that is ice free. Away from ice edges,  $k$  is an important control on  $F'$  in such locations as the tropical Pacific and the storm track of the North Atlantic (and to a lesser extent the Pacific). Here interannual variability in winds is considerable, probably associated with low-frequency modes of climate variability such as the El Niño–Southern Oscillation and the North Atlantic Oscillation (NAO), respectively.

Overall, this analysis yields findings that agree with many of those of *Doney et al.* [2009] insofar as that interannual variability in the global oceanic flux of  $\text{CO}_2$  is controlled primarily by  $\Delta p\text{CO}_2$  but that  $k$  contributes about 40% of this. In the following section, we build upon these findings, exploring the longer multiannual to multidecadal timescales of variability, with an emphasis on the North Atlantic.

#### 4.2. Critical Timescale of $\Delta p\text{CO}_2$ Dominance of $\text{CO}_2$ Flux Variability

In this section we identify at what timescale, if any, does variability in  $F$  become dominated by variability in  $\Delta p\text{CO}_2$ . To explore which parameters dominate flux variability over specific timescales, we average each component's contributions (i.e.,  $\Delta p\text{CO}_2' \bar{k} \bar{\alpha}$  for the contribution of  $\Delta p\text{CO}_2$ ) over various zonal areas to obtain mean contributions on the subbasin scale. We define zones as polar (Baffin Bay and the Greenland–Iceland–Norwegian, or GIN, Sea), subpolar ( $60^\circ\text{N}$ – $35^\circ\text{N}$ ), subtropical ( $35^\circ\text{N}$ – $10^\circ\text{N}$ ), and equatorial ( $10^\circ\text{N}$ – $10^\circ\text{S}$ ) (Figure 7a). We construct frequency spectra of these zonal mean contributions to quantify the energy of each contribution at specific timescales. Since the contributions from each component are in units of  $\text{CO}_2$  flux ( $\text{mmol m}^{-2} \text{ d}^{-1}$ ), one can compare their magnitudes directly. We also employ Welch's method of

segmenting signals to better constrain estimates of the spectra [Welch, 1967]. Briefly, this involves segmenting a signal into shorter segments of equal length, calculating the spectra of each segment and then averaging over all segments' spectra to obtain one more robust estimate of the spectrum. In our case, we segment the 150 year series of zonally averaged CO<sub>2</sub> flux anomalies and the contribution from  $k$  into five nonoverlapping segments of 30 year length. This method improves the confidence intervals of the spectrum calculated at the cost of being unable to solve for variability on timescales longer than the segment length. This is because the timescales of interest correspond to the lowest frequencies of variability, and so we plot the spectra in period space to highlight this end of the domain.

Across the North Atlantic, most of the variability in CO<sub>2</sub> flux is attributable to the contribution from either  $\Delta p\text{CO}_2$  or  $k$ ; the roles of  $\alpha$  and the cross terms are minor (not shown). Therefore, almost all of the spectral energy in CO<sub>2</sub> flux anomalies (Figures 7b–7e, blue lines) that does not correspond with the spectrum of  $k$  (red) is attributable to the contribution from  $\Delta p\text{CO}_2$ . In other words, where the energy in CO<sub>2</sub> flux anomalies is high, but the energy of  $k$ 's contribution is lower, most of the discrepancy comes from the contribution of  $\Delta p\text{CO}_2$ . In general, the long-period CO<sub>2</sub> flux variability comes from the variability of  $\Delta p\text{CO}_2$ , rather than  $k$ . We quantify the CO<sub>2</sub> flux variability that is dominated by the contribution from  $\Delta p\text{CO}_2$  as being the shortest period of variability where the amplitude of  $F'$  variability is at least twice as large as the contribution from  $k$  for all longer periods. A factor of 2 was chosen as it identifies the point at which a clear majority (at least half) of flux variability is attributable to the  $\Delta p\text{CO}_2$  contribution. To do this, we search along the spectrum from long to short periods for the first period where the spectrum of  $F'$  is equal to or less than double the energy of the contribution from  $k$ . The vertical dashed lines in Figures 7b–7e show the value of this critical timescale for each zonal band. If this number is small, then it means a wider band of long-period CO<sub>2</sub> flux variability is controlled entirely by  $\Delta p\text{CO}_2$ .

In the equatorial and subtropical latitudes, a very wide band of long-period variability in CO<sub>2</sub> flux is controlled by  $\Delta p\text{CO}_2$  (all timescales to the right of the vertical dashed lines in Figures 7c–7e). That is to say that the roles of  $k$  and  $\alpha$  are negligible for these long periods. The same is also true at subpolar latitudes, but the band of timescales is narrower: approximately decadal and longer-term variability in CO<sub>2</sub> flux is almost entirely controlled by  $\Delta p\text{CO}_2$ . The separation of the (95% confidence) error envelopes around the best estimates of the subpolar, subtropical, and equatorial spectra (darker blue and pink lines) indicate that the differences between the spectra at the large-period end are significant. For the polar zone, both  $\Delta p\text{CO}_2$  and  $k$  have an important role in driving flux variability for all timescales longer than interannual (even without curtailing the series length by segmentation), and so there is no long period dominated by  $\Delta p\text{CO}_2$ . In addition to the strong influence of  $\Delta p\text{CO}_2$ , there is also long-period variability in  $k$ . As  $k$  is scaled by sea ice cover, a negative trend in ice area (in response to a warming climate) will therefore force  $F'$  in the long term at high latitudes. Such a decline has been documented in this model setup [Yool *et al.*, 2013b]. Taken over the whole North Atlantic, we find that flux variability on pentadal and longer timescales is greatly dominated by the influence of  $\Delta p\text{CO}_2$ , and  $k$  contributes to less than quarter of long-period flux variability.

To more fully interpret the spectra of zonally averaged contributions, it is helpful to examine the critical timescale of  $\Delta p\text{CO}_2$  dominance at each grid point for the anthropogenic run (Figure 8a). At the grid point scale, one can infer which physical phenomena give rise to the spectra in Figure 7. The polar zone in both runs is dominated by points with no long timescale of  $\Delta p\text{CO}_2$  dominance: much of Baffin Bay and the western GIN Sea. These regions are strongly influenced by sea ice, but in the eastern ice-free GIN Sea long-period variability is dominated by  $\Delta p\text{CO}_2$ .

The subpolar zone features a southwest-to-northeast band of grid points whose flux variability is only dominated by  $\Delta p\text{CO}_2$  on multidecadal timescales (higher than elsewhere in the basin). This location coincides with the southern boundary of the NAC. Here there is long-period variability in wind speeds in the model, which drives the critical timescale of  $\Delta p\text{CO}_2$  dominance in the subpolar zone (~10 years) to be longer than the subtropical or equatorial zones (~3 and ~1 years, respectively).

We also estimate the critical timescale using observations in the three locations described in section 3. In the three 5-by-5° areas with the largest number of SOCAT monthly mean  $f\text{CO}_2$  values, we construct and decompose CO<sub>2</sub> fluxes using these  $f\text{CO}_2$  data (as in Figure 3), monthly mean CCMP winds, SST values from the EN4 gridded data set [Good *et al.*, 2013], and atmospheric  $p\text{CO}_2$  from Mauna Loa, Hawaii [Thoning *et al.*, 2014]. In these locations, there is a sufficient history of ocean  $f\text{CO}_2$  data to determine the critical timescale: 2 years in the subtropical box, 0.5 year in the midlatitude box, and 4 years in the high-latitude box (values shown as color

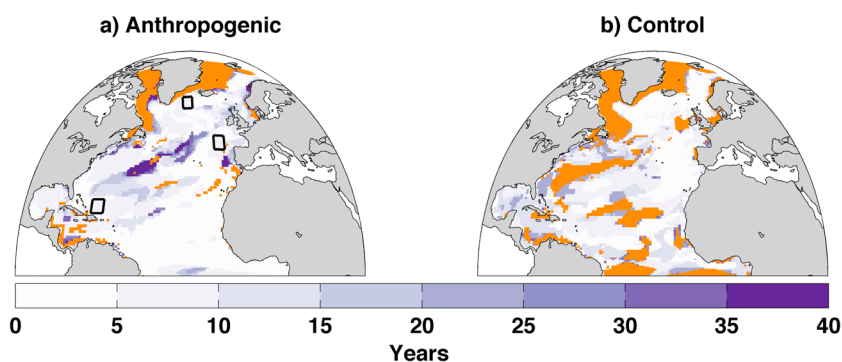


**Figure 8.** Largest timescale of  $\text{CO}_2$  flux variability for which the contribution of  $k$  is nonnegligible, beyond which variability is dominated by  $\Delta p\text{CO}_2$  for the (a) anthropogenic and (b) control runs. Shades of purple indicate this timescale, orange areas show where  $\Delta p\text{CO}_2$  never dominates on the longest timescales, and white non-Atlantic areas are out of bounds. Colors inside the three black squares in Figure 8a show the timescale derived using observations in the same locations as Figure 3 [CCMP winds *Atlas et al.*, 2011, SOCAT oceanic  $p\text{CO}_2$  *Bakker et al.*, 2014, MLO atmospheric  $p\text{CO}_2$  *Thoning et al.*, 2014, and EN4 SST *Good et al.*, 2013].

within black squares in Figure 8a). These values are comparable to those determined using model output in the same locations; 4.6, 3.7, and 4.6 years, respectively.

By examining the same metric for the control run, we can learn the extent to which  $\Delta p\text{CO}_2$  controls natural variability in the global ocean, without the influence of anthropogenic  $\text{CO}_2$  input. For much of the North Atlantic,  $\Delta p\text{CO}_2$  variability controls most of the  $\text{CO}_2$  flux variability in the control run (Figure 8b). Due to the construction of the control run, it is not possible to comment on variability on timescales longer than 30 years, yet this period is sufficiently longer than the  $\Delta p\text{CO}_2$  critical timescale for most of the ice-free North Atlantic. This means that natural, internal ocean multiannual  $\text{CO}_2$  flux variability is quite insensitive to the contribution from  $k$ , and therefore, that much of the control exerted by the  $\Delta p\text{CO}_2$  is not purely the product of anthropogenic emissions. In other words, the strong influence of the  $\Delta p\text{CO}_2$  in many parts of the North Atlantic is naturally occurring and not purely due to rising atmospheric carbon concentrations. Such variability in  $\Delta p\text{CO}_2$  may arise without a rise in atmospheric  $p\text{CO}_2$  due to ocean circulation (particularly horizontal and vertical advection). Advection acts to reorganize the surface inventories of heat, DIC, and alkalinity, thereby modulating ocean  $p\text{CO}_2$  [Doney *et al.*, 2009; Halloran *et al.*, 2015].

### 4.3. $\text{CO}_2$ Flux Estimation With Simplified $k$

Here we explore the extent to which flux variability can be reliably estimated in circumstances where we have a minimal knowledge of the variability in gas transfer velocity. In section 1, some of the uncertainties associated with  $k$  were outlined. A key question is understanding the extent to which those uncertainties limit our ability to estimate oceanic  $\text{CO}_2$  flux variability. We can approximate equation (11) by assuming that variations in the gas transfer velocity ( $k'$ ) and the role of the cross terms (terms 4 to 7) are small (demonstrated in section 4.2). Under these assumptions, terms 2, 4–7 vanish, yielding equation (13).

$$F' \approx \Delta p\text{CO}_2' \bar{k} \bar{\alpha} + \overline{\Delta p\text{CO}_2' k \alpha'} \quad (13)$$

If these assumptions are valid and equation (13) is a reasonable approximation, the uncertainties associated with  $k$  would also become irrelevant in the determination of flux variability. This estimation would be useful in estimating multidecadal flux variability using limited observations or simple box models. The “true” simulated  $\text{CO}_2$  flux is known in the model, and we are therefore able to determine the error due to the approximation in equation (13). By omitting some contributions, the estimated flux will necessarily have less variability than the actual flux. We therefore assess our estimation by quantifying at each grid point (1) the correlation coefficient ( $r$  values) between estimated and model actual fluxes that are significant beyond a level of 95% confidence and (2) the proportion of the flux variability that is captured by the estimation relative to the model’s actual flux variability. The error in observational reconstructions of  $\text{CO}_2$  flux is likely to differ due to the parameterization of gas transfer in the model, but the model validation (section 3) indicates that the statistical properties of the error should be similar on interannual to decadal timescales.

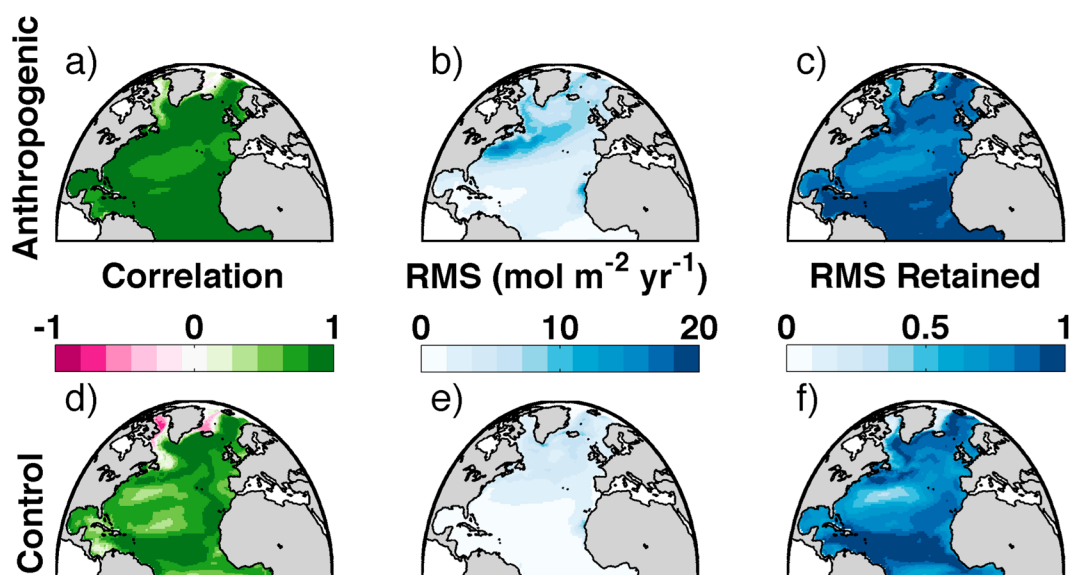


**Figure 9.** Evaluation of flux estimation applied to the (a–c) anthropogenic and (d–f) control runs, 1950–2099. Figures 9a and 9d show correlation between modeled and estimated fluxes (all values are of >95% significance). Figures 9b and 9e show RMS of modeled CO<sub>2</sub> flux anomalies (a measure of variability). Figures 9c and 9f show ratio between estimated and modeled CO<sub>2</sub> flux RMS (the proportion of variability captured by the estimation).

The longest-term variability in the North Atlantic CO<sub>2</sub> flux is primarily controlled by the positive trend in atmospheric pCO<sub>2</sub>. Correspondingly, the estimated CO<sub>2</sub> flux correlates very closely with the model's actual series (Figure 9a). However, even without this trend (as in the control run), the actual and estimated fluxes correlate well (Figure 9d). In general, the correlations are weaker in the control than in the anthropogenic run, and several local minima are apparent; these also correspond to regions where variability is generally small (Figures 9b and 9f). The good correlation between estimated and actual fluxes in both the anthropogenic and control runs suggests that the estimation captures the key patterns of flux variability, both anthropogenically and internally driven.

In addition to reproducing patterns of flux variability, it is also necessary for the estimation to correctly predict magnitudes. Since the estimation omits some contributions, it will naturally show either equal or lower variability than the actual flux. To quantify this, we show the ratio between the estimated and actual modeled CO<sub>2</sub> flux variability (as the RMS of monthly anomalies) (Figures 9c and 9f). Where the value is 1, the estimation reproduces all the modeled variability; values between 0 and 1 indicate the proportion of variability retained by the estimation. This metric indicates that the estimation is robust at reproducing most of the modeled variability across the Atlantic, in both the anthropogenic and control runs.

The main area where the flux estimation fares poorly is in the ice-covered North Atlantic. Here nonseasonal sea ice variability is an important control on fluxes. Our estimation implicitly excludes interannual variability in the ice edge and the multidecadal decline of ice extent, so the fluxes in the region are not well represented. To the south of the NAC there are local minima in correlations and the RMS is retained, which are more pronounced in the control run than the anthropogenic run. Although these areas are less well estimated than elsewhere in the Atlantic, the variability in these regions is small, and so flux variability on the basin and subbasin scale will still be well captured.

## 5. Discussion

Presently, large uncertainties are introduced into calculated CO<sub>2</sub> fluxes via the gas transfer velocity. The choice of wind speed parameterization can vary  $k$  by approximately 50% at global mean wind speeds (~7 m/s) and by 100% at speeds higher than 15 m/s [e.g., Woolf, 2005]. The choice of wind product can affect  $k$  by 10–40% [Wanninkhof *et al.*, 2002], and variability differs between products [Wanninkhof *et al.*, 2013; Wanninkhof, 2014; Kent *et al.*, 2013]. The roles of breaking waves and bubbles are not taken into account when using a purely wind speed-based parameterization of  $k$ , so these phenomena introduce poorly constrained uncertainty

[Prytherch *et al.*, 2010]. Certainly, these factors all limit our ability to accurately estimate CO<sub>2</sub> flux variability on interannual and shorter timescales, and ongoing work is needed in these areas.

In the high-latitude North Atlantic, the gas transfer velocity controls CO<sub>2</sub> flux variability on longer timescales than elsewhere in the basin. In the regions of the Labrador Sea, Baffin Bay, Denmark Strait, and Fram Strait, sea ice cover is an important mediator of gas exchange. Here long-period variability in sea ice cover controls CO<sub>2</sub> flux variability via the gas transfer velocity, since  $k$  is scaled by the fraction of area that is ice free. As a result, there is no long period of variability over which  $\Delta p\text{CO}_2$  predominantly controls the carbon flux. Therefore, to accurately quantify estimates of the high-latitude North Atlantic carbon flux, a detailed knowledge of sea ice dynamics is necessary.

Over the whole North Atlantic, pentadal and longer-term CO<sub>2</sub> flux variability is dominated by the influence of  $\Delta p\text{CO}_2$ . These longer timescales contrast the shorter timescales, where the role of  $k$  is crucial. This suggests that a detailed knowledge of the pentadal to multidecadal control of  $k$  on  $F$  may not be necessary to quantify the longer-term variability of the North Atlantic carbon sink. This finding therefore lends support to the approaches of studies such as that of McKinley *et al.* [2011], which attempt to make judgements about multidecadal variability of the North Atlantic CO<sub>2</sub> sink based purely on  $p\text{CO}_2$  observations. In their study, it was found that the oceanic trend in  $p\text{CO}_2$  converges to that of the atmosphere when examined over the full 29 year period between 1981 and 2009, but when only decadal timescales are considered, the two trends differ. Therefore, if on these same multidecadal timescales, the present day air-sea  $p\text{CO}_2$  difference is maintained as McKinley *et al.* [2011] suggest, then the North Atlantic CO<sub>2</sub> sink is approximately stable; neither a decline nor an enhancement of the flux is apparent. Our work would support this approach, since we find the roles of  $k$  and  $\alpha$  in governing flux variability over this timescale to be minor.

There is a broad increase in the critical timescale with latitude in the North Atlantic, which is explainable in terms of wind speed variability. At the low latitudes, wind speed variability is lower, increasing toward the poles (Figure 5). In addition, mean wind speeds are higher at the poles than the equator, so a given magnitude of wind speed variability at subpolar latitudes will produce greater variability in  $k$  than at the equator. This is because  $k$  scales with the square of the wind speed in our setup [Nightingale *et al.*, 2000]. This zonal increase in  $k$  variability, in addition to the presence of sea ice at the highest latitudes, is what causes the comparable zonal increase of the critical timescale (Figures 7 and 8). Furthermore, wind speed (and hence  $k$ ) variability is a stronger control on carbon fluxes in the control simulation than the anthropogenic run. This is because the control's fixed atmospheric CO<sub>2</sub> concentration means that there is much less variability in  $\Delta p\text{CO}_2$  (and therefore also in the CO<sub>2</sub> flux) than in the anthropogenic run. As a result, wind speed variability patterns become relatively more important in setting the critical timescale for the control run than the anthropogenic run (Figure 8). This means that  $k$  is a more important controller of variability of preindustrial carbon fluxes, although not more important than  $\Delta p\text{CO}_2$  on pentadal and longer timescales.

Through the comparison of modeled ocean  $f\text{CO}_2$  fields against observations from SOCAT and Bermuda, it was shown that our setup underestimates variability on timescales shorter than 1 year. This result is to be expected, since GCMs of this scale will tend not to represent high-frequency and small spatial-scale variability well [e.g., Taylor *et al.*, 2012]. This could indicate that the  $\Delta p\text{CO}_2$  contribution may be a stronger control on fluxes on shorter timescales than our study suggests. Our forcing set underestimates multiannual wind speed variability at high latitudes, which may be associated with an inability to appropriately represent the NAO (an issue common to many GCMs [Lee and Black, 2013]). This could cause the real-world critical timescale to be longer than what the model suggests. In the polar zone, the low bias does not affect the critical timescale, since  $k$  variability on all timescales is nonnegligible. In the subpolar zone, the critical timescale may be underestimated, due to the low bias, yet the observation-derived critical timescales are comparable to the model prediction ( $\sim 1$ –5 years for all three locations, using both model output and observations, Figure 8a).

Current ocean models (including NEMO-MEDUSA) do not derive  $k$  from the full range of kinetic factors that control it and instead parameterize it purely from wind speed. It is likely then that  $k$  variability on interannual and shorter timescales will be underestimated too; since real-world, shorter timescale variability in processes such as wave breaking and bubble dynamics is not represented in GCMs. Until a more thorough understanding of the mechanisms underlying  $k$  is developed, we will not know exactly how important it is in governing short-timescale flux variability. While the unmodeled factors are very likely strong controls on  $k$  on short timescales, it is not clear if their variability on longer timescales (decadal and longer) is large, relative

to the effect of wind speed. If on these long timescales  $k$  variability is dominated by the contribution from wind speed, then wind speed parameterizations of  $k$  should be sufficient to estimate decadal gas transfer variability.

It is worth exploring the caveat that we have derived our findings from GCM output. One could expect that other models and configurations would yield slightly different timescales for the emergence of  $\Delta p\text{CO}_2$  dominance of flux variability. Yet our choice of model and setup appears reliable for the purposes of our study. This experiment has been shown to produce interannual flux variability comparable to other models as well as observational estimates (Table 1). In addition, it captures real-world multiannual  $f\text{CO}_2$  variance (Figures 3 and 4) and a reasonable degree of wind speed variability (Figure 5) [Lee and Black, 2013]. Therefore, other models similarly capable of representing multiannual flux,  $f\text{CO}_2$ , and wind variability would likely give results consistent with those presented here, even if the mechanisms underlying that variability differ. Finally, the choice of gas transfer velocity parameterization can have some effect on the critical timescale derived. Functions [e.g., McGillis et al., 2001] that produce a wider range of  $k$  values over the most commonly occurring wind speed range (3 to 15 m/s) [Wanninkhof, 2014] impart greater variability into the  $\text{CO}_2$  flux and so would increase the critical timescale. Many of the most commonly used parameterizations, however, show the greatest concordance of derived  $k$  values over the range of commonly occurring wind speeds, and so the critical timescale is generally insensitive to the choice of function (see supporting information).

While we have clearly identified the roles of each of the components of the flux equation in governing  $F$  variability, our methodology only hints at which underlying processes are important. To derive a more complete and mechanistic understanding of the controls on carbon flux variability, further work is necessary. A very broad range of physical, chemical, and biological processes cause ocean  $p\text{CO}_2$  variability, and so future work should seek to quantify the relative importance of these drivers while attributing them to specific timescales of variability.

## 6. Conclusions

We have examined the relative importance of the three components of the air-sea  $\text{CO}_2$  flux equation ( $k$ ,  $\Delta p\text{CO}_2$ , and  $\alpha$ ) in controlling flux variability on a range of timescales. In the North Atlantic, as for much of the global ocean, we find that subannual to interannual variability in  $\Delta p\text{CO}_2$  and  $k$  both have important roles in controlling the air-sea carbon flux, in agreement with previous work [e.g., Doney et al., 2009]. On these timescales, it is critical to obtain estimates of  $\Delta p\text{CO}_2$  and  $k$  for accurate flux variability to be derived. On pentadal and longer timescales, variability in  $k$  is not important and can be ignored when estimating flux variability. The critical timescale increases from interannual at low latitudes to decadal at high latitudes.

## References

- Atlas, R., R. N. Hoffman, J. Ardizzone, S. M. Leidner, J. C. Jusem, D. K. Smith, and D. Gombos (2011), A cross-calibrated, multiplatform ocean surface wind velocity product for meteorological and oceanographic applications, *Bull. Am. Meteorol. Soc.*, *92*(2), 157–174.
- Bakker, D., et al. (2014), An update to the Surface Ocean  $\text{CO}_2$  Atlas (SOCAT version 2), *Earth Syst. Sci. Data*, *6*, 69–90.
- Bates, N., Y. Astor, M. Church, K. Currie, J. Dore, M. González-Dávila, L. Lorenzoni, F. Muller-Karger, J. Olafsson, and M. Santa-Casiano (2014), A time-series view of changing ocean chemistry due to ocean uptake of anthropogenic  $\text{CO}_2$  and ocean acidification, *Oceanography*, *27*(1), 126–141.
- Bates, N. R. (2007), Interannual variability of the oceanic  $\text{CO}_2$  sink in the subtropical gyre of the North Atlantic Ocean over the last 2 decades, *J. Geophys. Res.*, *112*, C09013, doi:10.1029/2006JC003759.
- Bender, M. L., S. Kinter, N. Cassar, and R. Wanninkhof (2011), Evaluating gas transfer velocity parameterizations using upper ocean radon distributions, *J. Geophys. Res.*, *116*, C02010, doi:10.1029/2009JC005805.
- Ciais, P., et al. (2013), *IPCC, 2013: Climate Change 2013: The Physical Science Basis. Contribution of Working Group I to the Fifth Assessment Report of the Intergovernmental Panel on Climate Change*, Cambridge Univ. Press, chap. 6 Carbon and Other Biogeochemical Cycles, Cambridge, U. K.
- Collins, W., et al. (2011), Development and evaluation of an Earth-System model—HadGEM2, *Geosci. Model Dev.*, *4*(4), 1051–1075.
- Doney, S. C., S. Yeager, G. Danabasoglu, W. G. Large, and J. C. McWilliams (2007), Mechanisms governing interannual variability of upper-ocean temperature in a global ocean hindcast simulation, *J. Phys. Oceanogr.*, *37*(7), 1918–1938.
- Doney, S. C., I. Lima, R. A. Feely, D. M. Glover, K. Lindsay, N. Mahowald, J. K. Moore, and R. Wanninkhof (2009), Mechanisms governing interannual variability in upper-ocean inorganic carbon system and air–sea  $\text{CO}_2$  fluxes: Physical climate and atmospheric dust, *Deep Sea Res., Part II*, *56*(8), 640–655.
- Frew, N. M., D. M. Glover, E. J. Bock, and S. J. McCue (2007), A new approach to estimation of global air-sea gas transfer velocity fields using dual-frequency altimeter backscatter, *J. Geophys. Res.*, *112*, C11003, doi:10.1029/2006JC003819.
- Good, S. A., M. J. Martin, and N. A. Rayner (2013), EN4: Quality controlled ocean temperature and salinity profiles and monthly objective analyses with uncertainty estimates, *J. Geophys. Res. Oceans*, *118*, 6704–6716, doi:10.1002/2013JC009067.
- Halloran, P. R., B. B. Booth, C. D. Jones, F. H. Lambert, D. J. McNeill, I. J. Totterdell, and C. Völker (2015), The mechanisms of North Atlantic  $\text{CO}_2$  uptake in a large Earth System Model ensemble, *Biogeosciences*, *12*(14), 4497–4508, doi:10.5194/bg-12-4497-2015.

### Acknowledgments

The authors are grateful for the input of two reviewers, whose feedback improved the clarity and strength of this manuscript. This work was supported the RAGNARoCC NERC directed research program (NE/K002546/1, NE/K00249X/1, and NE/K002473/1). The observational data used are available via the relevant references that accompany them in the text. The authors are very grateful to those who have produced and made freely available the CCMP, MLO Atmospheric  $\text{CO}_2$ , EN4, SOCAT, LDEO Flux Climatology, and BATS data sets. The Surface Ocean  $\text{CO}_2$  Atlas (SOCAT) is an international effort, endorsed by the International Ocean Carbon Coordination Project (IOCCP), the Surface Ocean Lower Atmosphere Study (SOLAS), and the Integrated Marine Biogeochemistry and Ecosystem Research program (IMBER), to deliver a uniformly quality-controlled surface ocean  $\text{CO}_2$  database. The many researchers and funding agencies responsible for the collection of data and quality control are thanked for their contributions to SOCAT. The model output used in this analysis is available as supporting information to this manuscript.

- Ho, D. T., R. Wanninkhof, P. Schlosser, D. S. Ullman, D. Hebert, and K. F. Sullivan (2011), Toward a universal relationship between wind speed and gas exchange: Gas transfer velocities measured with  $^3\text{He}/\text{SF}_6$  during the Southern Ocean Gas Exchange Experiment, *J. Geophys. Res.*, *116*, C00F04, doi:10.1029/2010JC006854.
- Jones, C., et al. (2011), The HadGEM2-ES implementation of CMIP5 centennial simulations, *Geosci. Model Dev.*, *4*(3), 543–570.
- Kent, E. C., S. Fangohr, and D. I. Berry (2013), A comparative assessment of monthly mean wind speed products over the global ocean, *Int. J. Climatol.*, *33*(11), 2520–2541.
- Khatiwala, S., F. Primeau, and T. Hall (2009), Reconstruction of the history of anthropogenic  $\text{CO}_2$  concentrations in the ocean, *Nature*, *462*(7271), 346–349.
- Landschützer, P., N. Gruber, D. Bakker, and U. Schuster (2014), Recent variability of the global ocean carbon sink, *Global Biogeochem. Cycles*, *28*, 927–949, doi:10.1002/2014GB004853.
- Le Quéré, C., J. C. Orr, P. Monfray, O. Aumont, and G. Madec (2000), Interannual variability of the oceanic sink of  $\text{CO}_2$  from 1979 through 1997, *Global Biogeochem. Cycles*, *14*(4), 1247–1265, doi:10.1029/1999GB900049.
- Lee, Y.-Y., and R. X. Black (2013), Boreal winter low-frequency variability in CMIP5 models, *J. Geophys. Res. Atmos.*, *118*, 6891–6904, doi:10.1002/jgrd.50493.
- Long, M. C., K. Lindsay, S. Peacock, J. K. Moore, and S. C. Doney (2013), Twentieth-century oceanic carbon uptake and storage in CESM1 (BGC), *J. Clim.*, *26*(18), 6775–6800.
- Madec, G. (2008), NEMO reference manual, ocean dynamics component: NEMO-OPA, Note du Pôle de Modélisation 27, Inst. Pierre Simon Laplace, France.
- Madec, G., and M. Imbard (1996), A global ocean mesh to overcome the North Pole singularity, *Clim. Dyn.*, *12*(6), 381–388.
- Martin, G. M., et al. (2011), The HadGEM2 family of Met Office Unified Model climate configurations, *Geosci. Model Dev.*, *4*(3), 723–757, doi:10.5194/gmd-4-723-2011.
- McGillis, W., J. Edson, J. Hare, and C. Fairall (2001), Direct covariance air-sea  $\text{CO}_2$  fluxes, *J. Geophys. Res.*, *106*(C8), 16,729–16,745.
- McKinley, G. A., M. J. Follows, and J. Marshall (2004), Mechanisms of air-sea  $\text{CO}_2$  flux variability in the equatorial Pacific and the North Atlantic, *Global Biogeochem. Cycles*, *18*, GB2011, doi:10.1029/2003GB002179.
- McKinley, G. A., A. R. Fay, T. Takahashi, and N. Metz (2011), Convergence of atmospheric and North Atlantic carbon dioxide trends on multidecadal timescales, *Nat. Geosci.*, *4*(9), 606–610.
- Myhre, G., et al. (2013), *IPCC, 2013: Climate Change 2013: The Physical Science Basis. Contribution of Working Group I to the Fifth Assessment Report of the Intergovernmental Panel on Climate Change*, Cambridge Univ. Press, chap. 8 Anthropogenic and Natural Radiative Forcing, Cambridge, U. K.
- Nightingale, P. D., G. Malin, C. S. Law, A. J. Watson, P. S. Liss, M. I. Liddicoat, J. Boutin, and R. C. Upstill-Goddard (2000), In situ evaluation of air-sea gas exchange parameterizations using novel conservative and volatile tracers, *Global Biogeochem. Cycles*, *14*(1), 373–387.
- Obata, A., and Y. Kitamura (2003), Interannual variability of the sea-air exchange of  $\text{CO}_2$  from 1961 to 1998 simulated with a global ocean circulation-biogeochemistry model, *J. Geophys. Res.*, *108*(C11), 3337, doi:10.1029/2001JC001088.
- Prytherch, J., M. J. Yelland, R. W. Pascal, B. I. Moat, I. Skjelvan, and M. A. Srokosz (2010), Open ocean gas transfer velocity derived from long-term direct measurements of the  $\text{CO}_2$  flux, *Geophys. Res. Lett.*, *37*, L23607, doi:10.1029/2010GL045597.
- Riahi, K., S. Rao, V. Krey, C. Cho, V. Chirkov, G. Fischer, G. Kindermann, N. Nakicenovic, and P. Rafaj (2011), RCP 8.5—A scenario of comparatively high greenhouse gas emissions, *Clim. Change*, *109*(1–2), 33–57.
- Rödenbeck, C., D. C. Bakker, N. Metz, A. Olsen, C. Sabine, N. Cassar, F. Reum, R. Keeling, and M. Heimann (2014), Interannual sea-air  $\text{CO}_2$  flux variability from an observation-driven ocean mixed-layer scheme, *Biogeosciences*, *11*, 4599–4613.
- Sabine, C. L., et al. (2004), The oceanic sink for anthropogenic  $\text{CO}_2$ , *Science*, *305*(5682), 367–371.
- Takahashi, T., et al. (2009), Climatological mean and decadal change in surface ocean  $\text{pCO}_2$ , and net sea-air  $\text{CO}_2$  flux over the global oceans, *Deep Sea Res., Part II*, *56*(8–10), 554–577, doi:10.1016/j.dsr2.2008.12.009, surface Ocean  $\text{CO}_2$  Variability and Vulnerabilities.
- Taylor, K. E., R. J. Stouffer, and G. A. Meehl (2012), An overview of CMIP5 and the experiment design, *Bull. Am. Meteorol. Soc.*, *93*(4), 485–498.
- Thoning, K., D. R. Kitzis, and A. Crotwell (2014), *Atmospheric Carbon Dioxide Dry Air Mole Fractions From Quasi-Continuous Measurements at Mauna Loa, Hawaii*, Natl. Oceanic and Atmos. Admin. (NOAA), Earth Syst. Res. Lab. (ESRL), Global Monit. Div. (GMD), Boulder, Colo.
- Timmermann, R., H. Goosse, G. Madec, T. Fichefet, C. Ethe, and V. Duliere (2005), On the representation of high latitude processes in the ORCA-LIM global coupled sea ice–ocean model, *Ocean Modell.*, *8*(1), 175–201.
- Wanninkhof, R. (1992), Relationship between wind speed and gas exchange over the ocean, *J. Geophys. Res.*, *97*(C5), 7373–7382.
- Wanninkhof, R. (2014), Relationship between wind speed and gas exchange over the ocean revisited, *Limnol. Oceanogr.*, *12*(6), 351–362.
- Wanninkhof, R., S. C. Doney, T. Takahashi, and W. R. McGillis (2002), The effect of using time-averaged winds on regional air-sea  $\text{CO}_2$  fluxes, in *Gas Transfer at Water Surfaces*, edited by M. A. Donelan et al., pp. 351–356, AGU, Washington, D. C.
- Wanninkhof, R., W. E. Asher, D. T. Ho, C. Sweeney, and W. R. McGillis (2009), Advances in quantifying air-sea gas exchange and environmental forcing, *Annu. Rev. Mar. Sci.*, *1*, 213–244.
- Wanninkhof, R., et al. (2013), Global ocean carbon uptake: Magnitude, variability and trends, *Biogeosciences*, *10*(3), 1983–2000, doi:10.5194/bg-10-1983-2013.
- Weiss, R. (1974), Carbon dioxide in water and seawater: The solubility of a non-ideal gas, *Mar. Chem.*, *2*(3), 203–215.
- Welch, P. (1967), The use of fast Fourier transform for the estimation of power spectra: A method based on time averaging over short, modified periodograms, *IEEE Trans. Audio Electroacoust.*, *15*, 70–73.
- Woolf, D. K. (2005), Parametrization of gas transfer velocities and sea-state-dependent wave breaking, *Tellus B*, *57*(2), 87–94.
- Yool, A., E. Popova, and T. Anderson (2013a), MEDUSA-2.0: An intermediate complexity biogeochemical model of the marine carbon cycle for climate change and ocean acidification studies, *Geosci. Model Dev.*, *6*, 1767–1811.
- Yool, A., E. Popova, A. Coward, D. Bernie, and T. Anderson (2013b), Climate change and ocean acidification impacts on lower trophic levels and the export of organic carbon to the deep ocean, *Biogeosciences*, *10*, 5831–5854.